TB18

19th International Symposium of Ballistics, 7–11 May 2001, Interlaken, Switzerland

BEHAVIOR AND PERFORMANCE OF AMORPHOUS AND NANOCRYSTALLINE METALS IN BALLISTIC IMPACTS

L. Magness[1], L.Kecskes[1], M.Chung[2], D. Kapoor[2], F. Biancianello[3], and S. Ridder[3]

[1] US Army Research Laboratory, Aberdeen Proving Ground, MD, 21005, USA
[2] US Army Research, Dev., and Eng. Center, Picatinny Arsenal, NJ, 07806, USA
[3] National Inst. Of Standards & Testing, Gaithersburg, MD, 20899, USA

Depleted uranium alloys that exhibit adiabatic shear localization and failure resulting in a self-sharpening mechanism offer superior armor penetration capability when compared to conventional tungsten heavy alloys. Both amorphous and nanocrystalline metals also exhibit shear banding deformation and failure mechanisms. Subscale ballistic tests are conducted with an amorphous metal alloy and a nanocrystalline tungsten-based composite. Penetration performances and the results of metallographic examinations of the residual penetrator debris are presented.

INTRODUCTION

When compared to tungsten heavy alloy (WHA) penetrators, the superior armor penetration capability of depleted uranium (DU) alloy penetrators, is attributable to DU's "self-sharpening" adiabatic shear (AS) mechanism [1]. In DU, thermal softening, due to the heat generated during high rate (effectively adiabatic) deformation of the penetrator, quickly overcomes work-hardening mechanisms. The plastic deformation of DU becomes unstable and tends to focus in plastic localizations known as (AS) bands [2]. AS banding is one of the few failure mechanisms that can operate under the hydrostatic pressures (approaching 6 GPa) in the head of the penetrator. This allows the DU penetrator to quickly discard the deforming material at its head, producing a sharpened or chiseled nose. By preventing the build-up of the large mushroomed heads observed on WHA penetrators, the AS failure mechanism allows a DU penetrator to efficiently burrow a smaller diameter (and therefore deeper) penetration cavity at a given impact velocity, or to perforate a given target at a lower impact velocity [1].

Efforts in the United States to develop alternatives to DU for penetrator applications have attempted to impart a similar deformation softening/shear localization behavior in WHAs [3, 4]. Conventional WHAs are two-phase composites of nearly unalloyed tungsten particles embedded in a nickel alloy matrix, produced by liquid-phase sintering of metal powders [5]. Because the tungsten phase itself is very resistant to AS localization, efforts have primarily focused on replacing the nickel alloy matrix with one having a

greater susceptibility to AS failure. A promising proof-of-principle for the approach was established with the use of DU as the replacement matrix [6]. Alternative (non-DU) matrices were selected on the basis of thermomechanical properties (such as low heat capacity, low work hardening, low strain rate sensitivity, and high thermal softening rate) that promote plastic instability and localization [2]. Ballistic evaluations have shown improvements in penetration behavior (greater susceptibility to shear localization), and significant improvements in penetration performance [7], however these novel tungsten composites have yet to equal the performance of the DU alloy (uranium with 0.75% titanium mass fraction) used in current US ammunition. Amorphous alloys and nanocrystalline alloys are now being examined also, as candidate penetrator materials or as the matrix alloy in novel tungsten-based composites, because of their unique shear banding deformation and failure mechanisms.

PROPERTIES OF AMORPHOUS AND NANOCRYSTALLINE MATERIALS

Nanocrystalline materials are generally defined as having an average grain size of less than 100 nanometers, while amorphous materials entirely lack the long-range atomic order of a crystalline structure. The mechanical properties of these materials differ fundamentally from their conventional crystalline counterparts.

At higher temperatures and moderate strain rates, both amorphous metals (also known as metallic glasses) and nanocrystalline materials can exhibit superplastic behaviors. At ambient temperatures, metallic glasses generally possess very high elastic strain limits (2 to 3%) and, therefore, very high yield strengths (between 1.6 GPa and 2.0 GPa). Beyond their elastic limits, however, the glasses do not exhibit strain hardening, and plastic deformation is immediately localized into shear bands. The localizations occur in quasi-static tests as well as dynamic tests. The localization is generally modeled as resulting from a reduction in local viscosity, associated with an increase in “free volume” as atoms move within the amorphous structure [8]. The nature of these localizations is still a very active area of research, but they do not appear to be thermally driven like the shear bands in DU. Many nanocrystalline alloys exhibit a similar, perfectly plastic and shear banding behavior in quasi-static and dynamic tests [9].

BALLISTIC TESTS OF AN AMORPHOUS METAL ALLOY

Until recently, amorphous metal alloys could be produced in only thin sections because cooling rates from the liquid metal exceeding 100,000 K/s were needed to avoid crystalline nucleation. The development of bulk amorphous metal (BAM) alloys reduced the required cooling rates to only 10 to 100 K/s and make it possible to produce BAM specimens with substantial dimensions (up to 5 cm thick) [10]. A key constituent in BAM alloys with the highest glass-forming abilities is beryllium; it is highly toxic as a metal or a metal oxide and thus a concern regarding the aerosols generated in ballistic impacts. New beryllium-free BAM alloys are being developed [11, 12]. Samples of one such alloy,

$Hf_{52.5}Ti_5Ni_{14.6}Cu_{17.9}Al_{10}$, were provided to the US Army Research Laboratory for ballistic tests by Todd Hufnagel of Johns Hopkins University (JHU).

The alloy was produced by arc melting the elemental constituents under an argon atmosphere. The melt was then quickly drawn into a cold copper mold to cast rods approximately 70 mm long and slightly over 3 mm in diameter. The alloy has a density of 11100 kg/m^3 (11.1 g/cm^3) and a yield strength of about 2.2 GPa [12]. The glass-forming ability of this alloy is not as good as the beryllium-bearing alloys, and small crystallites were observed in metallographic examinations (Fig. 1a).

Two subscale penetrators (3 mm in diameter by 60 mm in length) with masses of 4.76 g and 4.78 g, respectively, were machined from the small melt-cast rods and fired into steel targets. Both rods successfully survived launch from a smoothbore powder gun using a laboratory launch package (with a plastic sabot and obturator and a steel pusher disc). No residual stubs of penetrator were found in the penetration tunnels, but the eroded penetrator debris lining the tunnel were examined (Fig. 1 b and 2).

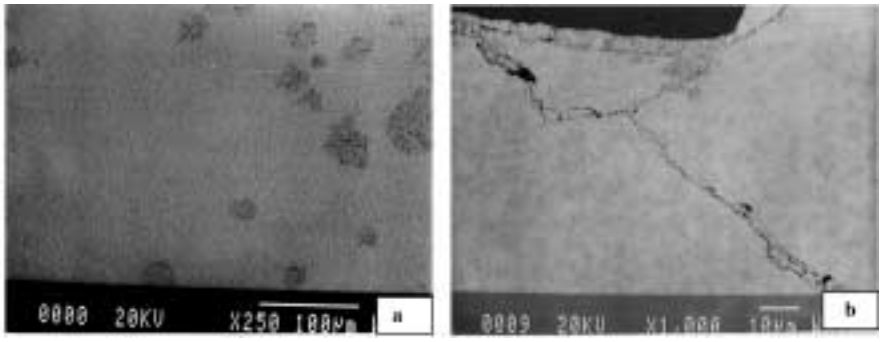

Figure 1. JHU penetrator material; (a) original as-cast microstructure of the glass with scattered crystallites in the amorphous phase, (b) dispersion of dendritic crystals within recrystallized penetrator residue.

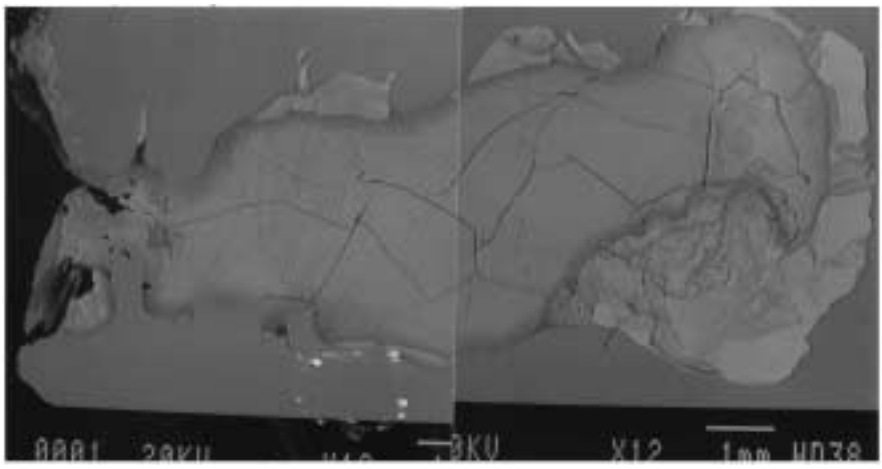

Figure 2. Roughened penetration tunnel displaced by JHU penetrator material, evidence of extensive melting of the penetrator and later formation of shrinkage cracks.

On a macroscopic scale (Fig. 2), the wall of the penetration tunnel had a roughened appearance, which is generally an indication that the penetrator had eroded or discarded material in a discontinuous process, and implies that localizations had developed in the deforming material at its head. Regions of apparently melted and heavily striated penetrator material, as well as fractured chips (Fig. 1b) are visible in the erosion products lining the tunnel wall. However, a close examination of the chips revealed a heterogeneous duplex structure with an isotropic dispersion of small dendritic crystals. This was unlike the original mostly homogeneous as-cast amorphous alloy (Fig. 1a). After the penetration event, localized heating most likely caused the penetrator material to melt and subsequently recrystallize under nonideal conditions.

BALLISTIC TESTS OF A NANOCRYSTALLINE TUNGSTEN COMPOSITE

A tungsten composite was produced in a two-stage ball milling process, – ball milling tungsten and nickel powders to produce agglomerated powders with nanocrystalline structures and then ball milling these powders with copper and aluminum powders. The powders were then consolidated in a hot isostatic press (HIP), at a pressure of 200 MPa at 950 ˚C, to form a tungsten composite with a density of 15200 kg/m^3 (15.2 g/cc) [13]. X-ray diffraction analyses indicated that average grain sizes grew during the consolidation, from under 100 nm in the powders, to 230 nm in the HIPed product.

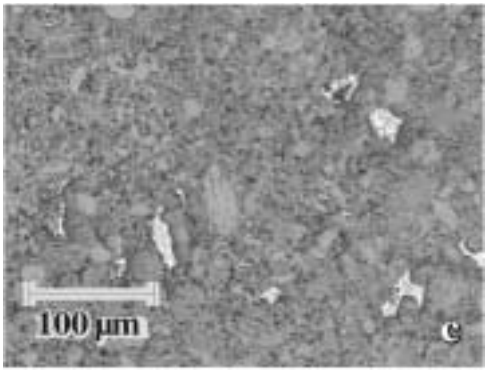

Figure 3. Microstructure of as-HIP consolidated W-Cu-Al-Ni, 200X.

The agglomerated, fully dense grains, as well as residual porosity, are visible in the HIP consolidated material under optical metallography (Fig. 3). The finer grained substructure is not visible. The only mechanical property characterizations performed on this material were Vickers Hardness tests (500 g load). The average reading was 717 HV_{500}, which corresponds to an approximate Rockwell "C" hardness of 59. Details of the processing history and material characteristics are given by Biancaniello et al. [13].

The ballistic behavior and performance of this material was compared to those of a conventional WHA with tungsten mass fraction of 90% (density of 17200 kg/m^3). Side-by-side tests, of quarter-scale rods of 65 g mass and length-to-diameter ratio of 15, deter-

mined limit velocities against a 3 in. (76.2 mm) Rolled Homogeneous Armor (RHA) plate at 0° obliquity (see Table 1).

Table 1. Ballistic Performance of Conventional and Nanocrystalline Tungsten-Composite Penetrators

Penetrator Material	Composition	Density (kg/m^3)	Limit Velocity vs. 76.2 mm RHA (BHN302)
Conventional WHA	90W-9Ni-1Co	17200	1390 m/s
Nanocrystalline W-composite	86W-12Cu-1.5Al-0.5Ni	15200	1347 m/s

With a density of only 15200 kg/m^3, penetrators of a conventional WHA would require velocities significantly higher (30–40 m/s estimated) than the 1390 m/s limit velocity of the 90% WHA against the RHA plate. Instead, the nanocrystalline tungsten composite delivered a limit velocity approximately 40 m/s below that of the conventional 90% WHA, which represents an approximate 6% reduction in the kinetic energy required to perforate the target. In a separate test, the nanocrystalline penetrator achieved a depth of penetration of 70.1 mm into a 150-mm-thick RHA plate at an impact velocity of 1396 m/s, slightly greater than that expected of a conventional WHA penetrator of the same density.

The nanocrystalline material displaced highly roughened penetration tunnels (Fig. 4a, 4b), suggesting that localizations had developed in the material. A large number of cracks were observed in the residual debris which lined the penetration tunnels, but their orientation (both radial and axial) suggest that these probably occurred during cooling of the erosion products, after the penetrator had come to rest in the target (Fig. 4b). The erosion products lining the penetration tunnel consist of chips of nanocrystalline penetrator material (Fig. 4b, 5a), divided by thick boundaries of apparently melted penetrator material. Most of the chips have rounded surfaces, implying frictional rubbing and heating between the chips. Within each of the chips, the material retained the original microstructure. All of these features are reminiscent of the features of DU erosion products (Fig. 5b), suggesting a very similar process of localization of the plastic deformation in the head of the penetrator, followed by the discard of discrete chips of material. Both of the ballistic results and the metallographic observations indicate that this nanocrystalline material's greater propensity for shear localization and failure improves its performance over that of conventional WHAs.

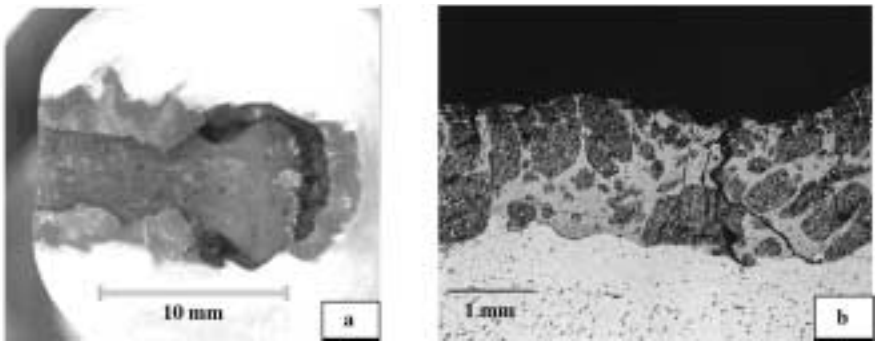

Figure 4. Residual penetrator and erosion products from nanocrystalline tungsten composite, (a) Roughened penetration tunnel, (b) Erosion products of chips and melted zones lining tunnel, note cracks formed upon cooling.

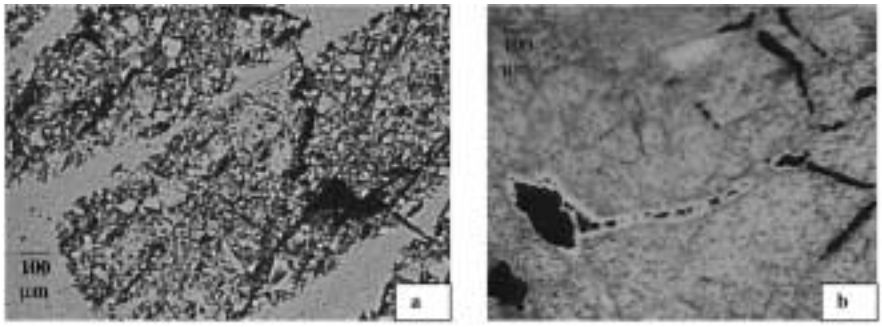

Figure 5. (a) Discrete chips of nanocrystalline tungsten composite penetrator material embedded in thick melted zones (50X), (b) Erosion products from uranium-3/4% titanium alloy penetrator, chips of moderately deformed material divided by adiabatic shear (white etching) bands (30X).

CONCLUSIONS

The limited results detailed above indicate that the inherent shear banding behaviors of nanocrystalline and amorphous materials offer some promise as re[lacements for DU, having the penetration capabilities similar to DU alloys, without the perceived hazards and political difficulties associated with DU. Both materials exhibit a process of localization of the plastic deformation in the head of the penetrator, resulting in the discard of discrete chips of material.

The great advantage of DU alloys results from their combination of mechanical and thermal properties that offer useful strength, ductility, and toughness at low to moderate strain rates, yet produce rapid plastic localization and failure under high rate loading (the adiabatic shear failure mechanism). This provides DU with the engineering properties required to survive the structural loads imposed during launch and penetrator interactions with complex armors (oblique spaced plate arrays or reactive sandwiches), while the adi-

abatic shear failures prevent the buildup of a large mushroomed head during armor penetration.

While DU develops the adiabatic shear failures only when the material is deformed to high strain rates (such as during the armor penetration process), amorphous and nanocrystalline metals develop shear bands immediately after the onset of plastic deformation, even at low strain rates. A challenge in the future will be to impart these materials with sufficient ductility and toughness to survive structural loads without overly delaying the shear localization and failure processes occurring during penetration.

REFERENCES

1. L. S. Magness and T. G. Farrand, "Deformation Behavior and Its Relationship to the Penetration Performance of High-Density Kinetic Energy Penetrator Materials", *Proceedings of the 1990 Army Science Conference*, 149–165, 1990
2. H. C. Rogers, "Adiabatic Plastic Deformation", *Ann. Rev. Material Sc.*, 9, 283–311, 1979
3. *Proc. of 1992 Int. conf. On Tungsten and Tungsten Alloys*, eds. A. Bose and R. Dowding, Metal Powder Industries Federation, 1993
4. *Proc. of 1994 Int. conf. On Tungsten and Tungsten Alloys*, eds. A. Bose and R. Dowding, Metal Powder Industries Federation, 1995
5. B. H. Rabin, A. Bose and R. M. German, "Characteristics of Liquid Phase Sintered Tungsten Heavy Alloys", *Int. J. Powder Met., 25*, No.1, 21–27, 1989
6. P. Dunn and B. Baker, "Target Penetrator Interaction: 70 Volume Percent Tungsten-30 Volume Percent Uranium Penetrator Material", *Proc. of 1st Int. conf. On Tungsten and Tungsten Alloys –1992*, 487–496, 1993
7. L. Magness and D. Kapoor, "Tungsten Composites with Alternative Matrices for Ballistic Applications", *Proc. of 2000 Int. Conf. On Tungsten, Hard Metals, and Refractory Alloys*, 15–23, 2000
8. F. Spaepen, "A Microscopic Mechanism for Steady State Inhomogeneous Flow in Metallic Glasses", *Acta. Met.*, 25, 407–415, 1977
9. J. E. Carsley, W. W. Milligan, S. A. Hackney and E .C. Aifantis, "Glasslike Behavior in a Nanostructured Fe/Cu Alloy", *Met. Trans. A*, 2479–2481, 1995
10. W.L. Johnson, "Bulk Glass-Forming Metallic Alloys: Science and Technology", *MRS Bulletin*, October 1999
11. X.H. Lin and W.L. Johnson, Mater. Trans., JIM, 38, 475, 1997
12. T. Hufnagel, Private communication, 10 Feb. 2000
13. F. S. Biancaniello, S. D. Ridder, M.E. Williams, R. D. Jiggetts, and L. S. Magness, "Characterization of Nanostructured Tungsten heavy Alloy Produced by Double Ball Milling," *Proc. of the Fourth Int. Conf. On Tungsten, Refractory Metal and Alloys – 1998*, Eds. A. Bose and R. J. Dowding, Orlando, FL, 1999